HHS Public Access

Author manuscript

Cancer Res. Author manuscript; available in PMC 2018 November 15.

Published in final edited form as:

Cancer Res. 2017 November 15; 77(22): 6097–6108. doi:10.1158/0008-5472.CAN-17-1018.

Cic loss promotes gliomagenesis via aberrant neural stem cell proliferation and differentiation

Rui Yang[1], **Lee H. Chen**[1], **Landon J. Hansen**[1], **Austin B. Carpenter**[1], **Casey J. Moure**[1], **Heng Liu**[1], **Christopher J. Pirozzi**[1], **Bill H. Diplas**[1], **Matthew S. Waitkus**[1], **Paula K. Greer**[1], **Huishan Zhu**[1], **Roger E. McLendon**[1], **Darell D. Bigner**[1], **Yiping He**[1,2], and **Hai Yan**[1,2]

[1]Department of Pathology and the Preston Robert Tisch Brain Tumor Center at Duke, Duke University Medical Center, Durham, NC, 27710

Abstract

Inactivating mutations in the transcriptional repression factor *Capicua* (*CIC*) occur in ~50% of human oligodendrogliomas (OD), but mechanistic links to pathogenesis are unclear. To address this question, we generated *Cic*-deficient mice and human OD cell models. Genetic deficiency in mice resulted in a partially penetrant embryonic or perinatal lethal phenotype, with the production of an aberrant proliferative neural population in surviving animals. *In vitro* cultured neural stem cells derived from *Cic* conditional knockout mice bypassed an EGF requirement for proliferation and displayed a defect in their potential for oligodendrocyte differentiation. *Cic* is known to participate in gene suppression that can be relieved by EGFR signal, but we found that *cic* also activated expression of a broad range of EGFR-independent genes. In an orthotopic mouse model of glioma, we found that *Cic* loss potentiated the formation and reduced the latency in tumor development. Collectively, our results define an important role for *Cic* in regulating neural cell proliferation and lineage specification, and suggest mechanistic explanations for how *CIC* mutations may impact the pathogenesis and therapeutic targeting of oligodendroglioma.

Keywords

CIC; EGFR; oligodendrocyte; OPC; differentiation; gliomagenesis; oligodendroglioma

Introduction

Oligodendrogliomas (OD) are a histologic type of diffuse glioma (WHO grade II–III) that account for between 5–20% of gliomas (1) and frequently display characteristic loss of whole chromosome arms 1p and 19q (1p/19q-codeletion) (2–4). Relative to other diffuse glioma subtypes, ODs are associated with better prognosis due in part to the tumor's increased chemo-sensitivity (5). However, tumor recurrence remains the most common cause of death for OD patients, as these tumors often recur or progress to higher grades. Previous studies from ours and other groups have revealed recurrent inactivating mutations

[2]Corresponding authors: Yiping He, Department of Pathology, Duke University Medical Center, DUMC-3156, 199A-MSRB, Research Drive, Durham, NC 27710. Phone: 919-684-4760; Fax: 919-684-8756; yiping.he@duke.edu; Hai Yan, Department of Pathology, Duke University Medical Center, DUMC-3156, 199B-MSRB, Research Drive, Durham, NC 27710. Phone: 919-668-7850; Fax: 919-684-8756; hai.yan@duke.edu.

of *Capicua* (*CIC*, on chromosome arm 19q) and *Far Upstream Element Binding Protein* (*FUBP1*, on chromosome arm 1p), identifying these genes as putative tumor suppressors for OD (6–9). Somatic mutations of these two genes, together with IDH1R1/2 mutations,1p/19q loss and *TERT* promoter mutations, define OD as a specific brain tumor subtype (6,7,10,11). Interestingly, whereas *TERT* promoter and *IDH* mutation occur across multiple diffuse glioma subtypes, somatic mutations of *CIC* and *FUBP1* are exclusively restricted to ODs, suggesting a possible link of *CIC* and *FUBP1* to oligodendrocyte lineage in neurogenesis and tumorigenesis.

CIC is a member of the Sox-related high-mobility group (HMG) subfamily and is highly conserved among species (12). Previous evidence suggests that Cic act primarily as a transcriptional repressor consisting of two highly conserved domains: the HMG-box which mediates DNA binding and nuclear localization, and a C-terminal motif C1 which co-operates with the HMG-box for DNA binding (12–16). In Drosophila, cic transduces the signaling of receptor tyrosine kinases (RTKs), Torso and the epidermal growth factor receptor (EGFR), and by doing so regulates cell proliferation and cell lineage specification during development (13,15,17–19).

Besides ODs, *CIC* is also linked to other cancers and non-cancer diseases in which its function as a transcriptional regulator is believed to be involved (14,20). However, the mechanism underlying the role of *CIC* inactivation in OD genesis remains unclear, in part due to the lack of appropriate animal and cell models of OD. In this study, we generated *Cic* knock-out mouse models, mouse neural stem cell (NSC) lines, and isogenic *CIC* knockout human OD cell lines to investigate the effect of *Cic* inactivation (loss) on neural development and on OD pathogenesis. We reveal aberrant neural development *in vivo* and defective NSC differentiation/proliferation *in vitro* upon *Cic* knockout, illuminate genes/pathways regulated by Cic via both EGFR-dependent and -independent mechanisms, and present direct evidence to support the tumorigenic role of *Cic* loss in OD genesis *in vivo*.

Materials and Methods

Generation of CIC$^{tm2a(KOMP)Wtsi}$ mice and *Cic*$^{flox/flox}$ mice

KOMP plasmid clone PRPGS00139_B_H08 was transfected into 129/B6 hybrid embryonic stem cells (ESCs) by electroporation (21). Targeted ESC clones were screened by polymerase chain reaction (PCR) and chimeric mice were generated by tetraploid blastocyst complementation performed by the Duke Transgenic Mouse Facility. F0 chimeric mice were further bred to C57BL/6 wildtype mice to generate F1 heterozygous *Cic*$^{tm2a(KOMP)Wtsi}$ mice (*Cic*$^{null/+}$). F1 mice were inbred to generate homozygous *Cic*$^{null/null}$ mice. In this case, viable homozygous *Cic*$^{tm2a(KOMP)Wtsi}$ offspring were under-represented due to the partial embryonic lethality. F1 mice were then bred to Flp-expressing mice (FLPo-10 from The Jackson Laboratory) to remove the Frt-flanked gene trap cassette in the *Cic*$^{tm2a(KOMP)Wtsi}$ allele, resulting in a conditional allele (*Cic*$^{flox/+}$) (21). Further inbreeding of these *Cic*$^{flox/+}$ mice allowed generation of homozygous *Cic*$^{flox/flox}$ mice, which allow further conditional knockout in the presence of Cre expression.

Genotyping

Tissue was lysed in lysis buffer (100mM Tris-HCl pH 8; 5mM EDTA pH 8; 0.2% SDS; 200mM NaCl; Proteinase K, and water) and DNA was ethanol precipitated. Pellet was re-suspended in 100 μl sterile H_2O. 1–2 μl of diluted DNA were used for PCR (15ul reaction volume). PCR was performed as followed: 95°C for 5 minutes, 30 cycles of (95°C for 15 seconds, 60°C for 15 seconds, 72°C for 15 seconds), 72°C for 5 minutes. Genotyping primers can be found in Supplementary Table S1. FFPE genomic DNA was extracted by the GeneRead DNA FFPE Kit (Quagen, Cat #180134) according to the manufacturer's instructions, and further genotyped to exclude chimeric expression of cic in brain tissue.

Mouse neonatal NSCs and virus transduction

Postnatal day 4 (P4) *Cic*$^{flox/flox}$ or *Cic*$^{+/+}$ neonatal mice were anesthetized by hypothermia and then decapitated with sharp scissors. The subventricular zone (SVZ) was micro-dissected from brains and dissociated into single cells by trituration. These cells were then cultured as neurospheres in EGF/FGF containing serum-free neural stem cell medium (Stemcell Technologies, Cat#05702) following the manufacturer's instructions. To obtain *Cic*$^{-/-}$ NSC lines, *Cic*$^{flox/flox}$ NSC lines were transduced with Cre-expressing adenovirus (vectorbiolabs, cat#1769) at a MOI of 10–100. Removal of the stop cassette was verified by PCR. *Cic*$^{+/+}$ NSC lines were similarly transduced with the Cre-expressing adenovirus and served as the control (*Cic*$^{+/+}$ NSC lines). These cells were used for all *in vitro* assays (proliferation assay, drug resistance assay, and microarray).

In vitro differentiation of NSCs and immunofluorescent staining

Cic$^{-/-}$ or *Cic*$^{+/+}$ NSCs were cultured for 7 days in 8 chamber vessel glass slides (BD Falcom, ref# 354108) in either complete proliferation medium (Stemcell Technologies, Cat#05702) supplemented with EGF (20ng/ml) and FGF (10ng/ml) or differentiation medium (Stemcell Technologies, Cat#05704). Cells were fixed by formalin, blocked with blocking buffer (1%BSA,10% goat serum in PBS), and stained with the following primary antibodies: Nestin (Stemcell Technologies, Cat#60051, 1:50), GFAP (Stemcell Technologies, Cat#60048, 1:200 or Cell Signaling Cat#12389, 1:100), Olig2 (Millipore, Cat#AB9610, 1:100), Ki67 (BD, Cat#550609, 1:100), β3 tubulin (Stemcell Technologies, Cat#01409, 1:1000), or CNPase (Cell Signaling Cat#5664, 1:100). After blocking with primary antibodies, cells were washed 3 times in PBS and stained with appropriate Alexa Fluor secondary antibodies (1:500) for 30 minutes at room temperature. Cells were washed with PBS and counterstained with DAPI before being mounted with mounting medium (Vectashield H-1400). Slides were imaged with a Nikon ECLIPSE TE2000-E fluorescent microscope.

In vitro proliferation assay and drug study

Cells were plated on laminin-coated 96-well plates at a density of 1000–3000 cells/well. At designated time points, CCK8 reagent (Dojindo, CK04-20) was added into each well according to manufacturer's instructions. After incubation for 3–5 hours, OD450 absorbance of each well was screened by a microplate reader (Tecan, infinite M200PRO). For cell

response to U0126, cells were plated out for 24 hours before U0126 was added into the wells.

Gene expression microarray analysis

Four *Cic*$^{+/+}$ and three *Cic*$^{-/-}$ neonatal NSC lines (established from different animals independently) were cultured in 6-well plates in the standard proliferation medium (Stemcell Technologies, Cat#05702) with or without EGF (20ng/ml) for 24 hours. RNA was then extracted by RNA miniprep kit (Zymo, Cat# 11-328) following the manufacturer's instruction and submitted to Duke Sequencing and Genomic Technologies Shared Resource for microarray hybridization (Affymetrix GeneChip MO 2.0 ST, Cat#902118). Gene expression microarray data has been submitted the Gene Expression Omnibus (GEO) database under accession GSE95012. The Robust Multichip Average (RMA) method was applied for data processing and normalization by R. For the most differentially expressed genes in response to EGF depletion, fold changes of gene expression (EGF- vs. EGF+) of both *Cic*$^{+/+}$ and *Cic*$^{-/-}$ cells were calculated and averaged (designated as fold change 1 and fold change 2), and difference of fold changes 1 and 2 (Δfold change) were calculated. Most differentially expressed genes in *Cic*$^{-/-}$ versus *Cic*$^{+/+}$ NSCs in response to EGF depletion were selected if Δfold change (log2-ratio) was equal or greater than 1. The enrichment score is −log(p-value or EASE score). EASE score (or p-value) is a modified Fisher's exact test calculated by the same method as pathway analysis by DAVID (22). To Stratify genes regulated differently by EGFR and/or *Cic*, genes with expression absolute fold change by EGF (EGF- vs. EGF+, in *Cic*$^{+/+}$ cells) equal or greater than 2 and absolute fold change by Cic (*Cic*$^{-/-}$ vs. *Cic*$^{+/+}$) in EGF-depleted condition equal or greater than 2 were defined as EGF-regulated Cic downstream targets (group I, 44 genes); genes with expression absolute fold change by EGF (EGF- vs. EGF+, in *Cic*$^{+/+}$ cells) equal or greater than 2 and absolute fold change by Cic (*Cic*$^{-/-}$ vs. *Cic*$^{+/+}$) in both EGF+ and EGF-depleted conditions smaller than 2 were defined as non-Cic-related EGF downstream targets (group II, 183 genes); genes with expression absolute fold change by Cic (*Cic*$^{-/-}$ vs. *Cic*$^{+/+}$) in EGF-depleted condition equal or greater than 2 and absolute fold change by EGF (EGF- vs. EGF+, in both *Cic*$^{+/+}$ and *Cic*$^{-/-}$ cells) smaller than 2 were defined as non-EGF-regulated Cic downstream targets (group III, 192 genes). Cell type-specific genes are defined according to http://www.stanford.edu/group/barres_lab/brain_rnaseq.html (23). Fold enrichment of astrocytes, neurons, newly formed oligodendrocytes, myelinating oligodendrocytes, OPC, microglial and endothelial cells are calculated as FPKM of one cell type divided by average of FPKM of all other cell types. Top 500 candidate genes of each cell type were documented. Genes specific to "newly formed oligodendrocytes" and "myelinating oligodendrocytes" are merged as "oligodendrocytes" for simplicity.

Generation of isogenic *CIC* knockout HOG cell lines by CRISPR-Cas9

A human oligodendroglioma cell line (HOG) was cultured in Iscove's Modified Dulbecco's Medium (IMDM) (Gibco, Invitrogen) supplemented with 10% FBS as previously described (24). This cell line is wild type in both IDH1 and IDH2 genes and does not have 1p/19q co-deletion. The CRISPR/Cas9 system was used for gene editing. pSpCas9(BB)-2A-GFP (PX458) was a gift from Feng Zhang (Addgene plasmid #48138) (25). Double-stranded oligonucleotides were cloned into restriction enzyme BbsI-linearized PX458 to construct

plasmids for CRISPR/Cas9 targeting of human *CIC*. Three individual sgRNA sequences targeting human CIC were designed with optimal targeting efficiency and minimal off-targets (26,27), and one non-targeting sequence (NTC) (28) was used as a negative control. The sequences of the sgRNAs are: sgRNA-e1: gctactgaccgaacatgccg, sgRNA-e4: ctctaccgcccggaaaacgt, sgRNA-e13: agagctcgtgggcccgtacg, sgRNA-NTC: gtatcctgacctacgcgctg. For targeting CIC, three different combinations of sgRNAs (e1+e4, e1+e13, e4+e13) were used for gene knockout via allele deletions or indels. For transient plasmid transfection, plasmids (two plasmids at 1:1 ratio for achieving the desired gene deletion/mutations) and Transfex (ATCC, cat# ACS-4005) were mixed and used for cell transfection according to manufacturer's instructions. One to three days after the transfection, GFP+ cells were sorted via fluorescence-activated cell sorting (BD FACSVantage SE cell sorter, Duke Cancer Institute) to obtain a GFP+ population to enrich transfected cells. These cells were further cultured for one to three days allowing them to recover from the FACS sorting and then serially diluted in 96-well plates for generating single-cell clones. Clones were screened for inactivating alterations by Sanger sequencing. Four subclones bearing different homozygous nonsense mutations in CIC were identified and numbered as HOG_1, HOG_2, HOG_3, and HOG_4, respectively. Ablation of CIC protein level (both long isoform of CIC, CIC-L and short isoform of CIC, CIC-S) was validated by CIC western blot (NOVUS, Cat# NB110-59906, 1:1000). STR profiling was performed by the Cell Culture Facility at Duke to validate that the four isogenic *CIC* knockout lines have consistent STR profiling with the parental line.

ChIP-Seq and data analysis

Chromatin immunoprecipitation was performed as previously described (29). Briefly, cells were cross-linked and cell lysate was then prepared and subjected to sonication to shear the chromatin. Protein G magnetic beads (New England BioLabs, Cat# S1430S) conjugated with anti-CIC antibody (NOVUS, Cat# NB110-59906) were used for immunoprecipitation. ChIP-derived DNA was recovered for library preparation. High-throughput sequencing (Illumina HiSeq 4000 system) was performed by Duke Sequencing and Genomic Technologies Shared Resource, and data analysis was performed by Duke Genomic Analysis and Bioinformatics Shared Resource. Reads were mapped to GRCh37 version of the human genome using the Bowtie alignment algorithm (30). For the aligned data, signal tracks were generated according to the calculation of the log 10 likelihood ratios between CIC wild type line ChIP-seq signal and two controls (IgG control and CIC knockout cell line control, respectively) by MACS2 2.1.1. Narrow regions of enrichment were identified using MACS2 2.1.1 with the fragment size of 300 bp based on wet experiment results and the q-value cut-off as 0.05 (http://github.com/taoliu/MACS/) (31). ChIP-seq signal track was visualized by the Integrative Genomics Viewer (IGV) (32,33). Peak location data was annotated by PAVIS (34).

Gliomagenesis modelling via orthotopic implantation of NSCs

$Cic^{-/-}$ and $Cic^{+/+}$ NSC lines (one line for each genotype) were transduced with retrovirus expressing human platelet-derived growth factor subunit B (*PDGFB*). The retrovirus construct, MigR1-*PDGFB*, co-expresses GFP and *PDGFB* from the same transcript via an internal ribosomal entry site (IRES) (Addgene #27490) (35). MigR1-*PDGFB* retrovirus

particles were produced in 293FT cells, and used to transduce NSCs at a MOI of 10–100. Transduced NSCs were further sorted by fluorescence-activated cell sorting (BD FACSVantage SE cell sorter, Duke Cancer Institute) for GFP positive cells. The resulting GFP+/*PDGFB*-expressing $Cic^{-/-}$ or $Cic^{+/+}$ NSCs were injected intracranially into the right striatum of 4–6 week old NSG mice at a dose of 250,000 cells per mouse. Mice were sacrificed when they showed signs or symptoms of brain abnormalities such as macrocephaly or lethargy. Brains were harvested, formalin-fixed and embedded in paraffin for subsequent immunohistochemistry and immunofluorescent staining assays.

TCGA Data Analysis

All TCGA gene expression data was downloaded from the online portal, https://gdc-portal.nci.nih.gov/. *CIC* copy number and mutation status, as well as *IDH1/2* mutation status and histologic subtype were retrieved from cbioportal (36,37), and matched to cases with gene expression data available. The 2016 TCGA Merged Glioma cohort was used for all analyses (38). All patient cases with complete information available (i.e., confirmed genotype of *IDH*, *CIC*) were used for each analysis unless otherwise stated, which consisted of 100 oligodendroglioma patients. 748 genes were generated for heatmap by using a t test to compare expression levels of each gene between $CIC^{-/-}$ and $CIC^{+/-}$ cases and filtering for all genes with a t test p value $<2.5\times10^{-3}$.

Statistical analysis

Quantification of Olig2+ cells in the adult survival $Cic^{+/+}$ and $Cic^{-/-}$ mice were manually performed using two slides from each animal (n=2 for each genotype) and a two-tailed unpaired Student's *t*-test was used to assess significant differences between conditions. For all *in vitro* proliferation assays by CCK8, at least two independent cell lines of each genotype were included and experiments were conducted at least twice. Two-tailed unpaired Student's t-test analysis was performed to compare the $Cic^{-/-}$ lines to the control lines (three technical replicates were performed for each line). QPCR for gene expression analysis was performed with two technical replicates and the ΔΔCt method to determine normalized gene expression. For Kaplan-Meier curve, log-rank test p value was calculated. For all microarray data analysis, expression absolute fold change cutoff was set to equal or greater than 2. For all experiments, error bars represent ± standard error; *p<0.05, **p<0.01, ***p<0.001.

Ethics statement

All animal studies were approved by the Duke Institutional Animal Care and Use Committee, an institution accredited by the Association for Assessment and Accreditation of Laboratory Animal Care (AAALAC), International. Protocol number: A072-13-03 and A037-16-02.

Results

Knockout of *Cic* results in aberrant hyper-proliferative cells in the adult SVZ

Previous studies have revealed the essential role of *CIC* in development and the neurodegeneration disorder SCA1 in humans (20). To determine the effects of a *Cic* inactivation in neural development, we generated a *Cic* knockout mouse model using a

targeting plasmid, *Cic*$^{tm2a(KOMP)Wtsi}$ (Fig. 1A; Supplementary Fig. S1A) (21). Heterozygous founder mice were crossed to obtain homozygous *Cic* knockout progeny in which both alleles are *Cic*$^{tm2a(KOMP)Wtsi}$ (abbreviated as *Cic*$^{null/null}$ hereafter) (Supplementary Fig. S1B). In addition, conditional knockout *Cic*$^{flox/flox}$ mice can be generated by breeding F1 mice to Flp-expressing mice (Fig. 1A; Supplementary Fig. S1C). Among 80 live pups, only six (7.5%) of them, including one runt which died shortly after birth, were homozygous knockout, likely due to a partial embryonic or perinatal lethality in *Cic*$^{null/null}$ animals.

We first determined the effect of *Cic* knockout on neural development by examining the brain from viable, postnatal *Cic*$^{null/null}$ animals. As expected, at postnatal day 4 (P4), both wildtype control (*Cic*$^{+/+}$) and *Cic*$^{null/null}$ mice displayed active postnatal neurogenesis, as validated by the expression of Ki67 around the lateral ventricles (Supplementary Fig. S2). By P28, while Ki67 expression was no longer detected in the SVZ in wildtype animals, as expected (39), active cell proliferation (Ki67 positive) was readily detectable in *Cic*$^{null/null}$ mice (Fig. 1B). Furthermore, the population of GFAP-expressing cells was greatly elevated in the SVZ of *Cic*$^{null/null}$ mice compared to those in the wildtype mice (Fig. 1C). As GFAP-expressing type B radial cells represent the dominant NSC population in the SVZ (40), these results suggest *Cic* loss leads to an aberrant hyper-proliferative population in the adult SVZ. Consistent with these hyper-proliferative phenotypes, DAPI staining of the brain tissue sections at similar planes revealed thicker lateral ventricular walls in *Cic*$^{null/null}$ mice compared to those in *Cic*$^{+/+}$ mice (Fig. 1D). Finally, while no differential expression of Nestin or Sox2 were observed in the SVZ of *Cic*$^{+/+}$ and *Cic*$^{null/null}$ mice, there was a significantly increase in the number of cells expressing Olig2 (Olig2+) in the dorsal part of lateral septal nucleus (LSD) of *Cic*$^{null/null}$ mice (Figs. 1E and 1F), suggesting an aberrant expansion/migration of the oligodendrocyte progenitor cells (OPC) and providing a potential link between *Cic* inactivation and oligodendrocyte differentiation. Collectively these results suggest that *Cic* inactivation results in aberrant development/expansion of cell populations in the adult SVZ, reminiscent of a pre-neoplastic phenotype.

Cic$^{-/-}$ NSCs bypass the requirement of EGF for proliferation under hypoxia condition

The observed pre-neoplastic phenotype raises the possibility that *Cic* knockout leads to aberrant proliferation of NSCs and/or other neural lineage progenitor cells. To overcome the high mortality seen in generating *Cic*$^{null/null}$ animals, we crossed the F1 mice (*Cic*$^{null/+}$) with FLPase-transgenic mice (FLPo-10 from the Jackson Laboratory) to achieve Flp-mediated deletion of the gene trap cassette. These resultant mice contained functional *Cic* alleles (*Cic*^{flox}), which allowed for subsequent, Cre recombinase-induced *Cic* knockout (Fig. 1A). NSC cell lines were established from the SVZ of P4 *Cic*$^{+/+}$ or *Cic*$^{flox/flox}$ mice followed by adenovirus-mediated transient Cre expression, resulting in the generation of *Cic*$^{-/-}$ NSC lines (Supplementary Fig. S1C).

We first analyzed the proliferation of NSCs and found that under the standard NSC proliferation medium condition (EGF-supplemented, normoxic culture), both *Cic*$^{+/+}$ and *Cic*$^{-/-}$ NSCs propagated robustly. As expected, the growth of the NSCs was dependent on the EGFR signaling, as withdrawal of EGF from the proliferation medium greatly attenuated the expansion of the NSCs, regardless of their *Cic* status (Supplementary Figs. S3A and

S3B). Although hypoxia in most cases is considered to play an important role in pathological conditions such as tumorigenesis, it is also well established that a physiological gradient of oxygen exists in the central nervous system (CNS) and that mild hypoxia is a physiological condition in normal brains (41). We therefore tested the proliferation of NSCs under a mild hypoxic culture environment (3% oxygen). We found that under the standard, EGF-supplemented proliferation media, both $Cic^{+/+}$ and $Cic^{-/-}$ NSCs again propagated robustly (Figs. 2A and 2B). However, when EGF was withdrawn from the media, a striking difference in response was observed: while the growth of $Cic^{+/+}$ NSCs was completely attenuated, the growth of $Cic^{-/-}$ NSCs was barely affected by the EGF withdrawal (Figs. 2A and 2B; Supplementary Figs. S3C and S3D). In agreement with this resistance to EGF withdrawal, $Cic^{-/-}$ NSCs were more resistant to U0126, an inhibitor of the downstream kinase of EGFR signaling, MEK (Fig. 2C). These results are consistent with previous findings showing that *cic* acts as a downstream mediator of the EGFR signaling pathway (13,17,19). Additionally, they provide one potential mechanism underlying the aberrant proliferation of NSCs *in vitro* and the pre-neoplasia we observed *in vivo*. The EGF-independent growth of $Cic^{-/-}$ NSCs under the mild hypoxic condition is particularly interesting as hypoxia/oxygen concentration is a prominent factor in both physiological and tumorigenic conditions in the CNS (41,42).

$Cic^{-/-}$ NSCs have a compromised oligodendrocyte differentiation potential and are arrested in an OPC-like state

The aberrant NSC proliferation observed in the above models, together with the knowledge that *CIC's* inactivating mutations predominantly occur in human ODs (6–9), prompted us to investigate the effect of *Cic* knockout on neural lineage specification. To evaluate the differentiation potential of $Cic^{+/+}$ and $Cic^{-/-}$ NSCs, we cultured these NSCs under the aforementioned mild hypoxic conditions in the standard NSC proliferation media, or in the differentiation medium. As expected, under the proliferation conditions, immunostaining of protein markers revealed that both $Cic^{+/+}$ and $Cic^{-/-}$ NSCs positively expressed Nestin and Olig2 (Supplementary Fig. S4A). Furthermore, both NSCs had no detectable expression of GFAP, Tuj1, and CNPase, which are differentiation markers for mature glial cells, neurons and oligodendrocytes, respectively, confirming their neural stemness/undifferentiated state. After being cultured in differentiation medium for 7 days, both $Cic^{+/+}$ and $Cic^{-/-}$ cells lost Nestin expression and displayed strong GFAP expression in the majority of the cells. This suggests that both $Cic^{+/+}$ and $Cic^{-/-}$ NSCs were readily able to differentiate to glial-like cells (Supplementary Fig. S4B). Interestingly, in response to the differentiation stimulus, while there were only about 4% of $Cic^{+/+}$ cells expressing Olig2 (an OPC marker), a significantly higher percentage (around 30%) of $Cic^{-/-}$ cells retained Olig2 expression (Figs. 3A and 3B, $p<0.001$). Furthermore, while cells positively expressing CNPase, a mature oligodendrocyte marker, were readily detected in the $Cic^{+/+}$ cultures, they were barely detectable in the $Cic^{-/-}$ cultures, even after 7 days of differentiation (Fig. 3C; Supplementary Fig. S5), suggesting that upon differentiation induction, $Cic^{-/-}$ NSCs are unable to differentiate into mature oligodendrocytes and instead blocked in an OPC-like stemness state.

We next performed gene expression profiling analysis to examine how these NSCs may respond differently to the presence/absence of the EGFR signal. Four independent *Cic*$^{+/+}$ and three independent *Cic*$^{-/-}$ NSC lines were cultured in proliferation medium with or without EGF for 24 hours before being harvested for gene expression profiling analysis. Knocking out of Cic transcript was further validated by QPCR (Supplementary Fig. S6A). We found that in the control, *Cic*$^{+/+}$ NSCs, the withdrawal of EGF (i.e., the absence of EGFR signaling) from the proliferation medium led to the upregulation of lineage differentiation markers, including those of oligodendrocytes, astrocytes and neurons. This is consistent with previous evidence that withdrawal of mitogen triggers lineage differentiation of NSCs. Interestingly, when *Cic*$^{-/-}$ NSCs were subjected to the same EGF withdrawal condition, a different gene expression pattern was observed: the top genes that displayed the most distinct expression pattern from that of *Cic*$^{+/+}$ NSCs were enriched for oligodendrocyte differentiation genes, and the expression of these genes were no longer upregulated in *Cic*$^{-/-}$ cells upon EGF depletion (Fig. 3D; Supplementary Fig. S6B). In particular, among the 73 genes showing the most distinct response to EGF depletion in *Cic*$^{-/-}$ NSCs versus in *Cic*$^{+/+}$ NSCs, 37 of them are well-established neural lineage markers as defined by previous studies (23,43). Among them, 10 are OPC markers and 18 are oligodendrocyte markers, including *Myrf*, a master regulator of oligodendrocyte differentiation (44), while only 2 are astrocyte markers and 7 are neuron markers. The 18 oligodendrocyte marker genes (such as *Enpp6*, *Plp1*, *Mag* and *Myrf*) were all upregulated in *Cic*$^{+/+}$ NSCs in response to EGF-depletion, but displayed no or barely any differential expression in *Cic*$^{-/-}$ NSCs under the same experimental condition. A distinct trend was also observed for the 10 OPC marker genes: 6 out of the 10 OPC marker genes were upregulated in *Cic*$^{-/-}$ cells, including the well-studied OPC marker gene *Pdgfra,* but showed no such trend of expression upregulation in *Cic*$^{+/+}$ cells (Supplementary Fig. S6C). These findings support a compromised oligodendrocyte differentiation program in *Cic*$^{-/-}$ NSCs (Fig. 3E), and suggest that besides providing an aberrant mitotic signaling, *Cic* loss leads to a compromised capability of NSCs to differentiate into mature oligodendrocytes; instead, these *Cic*$^{-/-}$ cells more likely possess OPC-like stemness, a finding that is consistent with the aberrant OPC-like population observed *in vivo*, and supports the exclusive link between *CIC* mutation and human ODs.

Cic regulates expression of novel downstream target genes that are independent of EGFR signaling

The aberrant differentiation/propagation phenotypes of *Cic*$^{-/-}$ NSCs led us to further examine the aforementioned gene expression profiles. We identified three groups of genes which were distinctly regulated in response to EGF depletion and by *Cic* status (Fig. 4A; Supplementary Table S2). The genes in the first group (group I, 44 genes) are EGF-regulated Cic downstream targets. These genes are regulated by EGF in *Cic*$^{+/+}$ NSCs but become no longer or less responsive to EGF in *Cic*$^{-/-}$ NSCs. This is consistent with the well-established function of Cic as a downstream mediator of EGFR signaling (13,17,19). It is worth noting that 28 of these 44 genes are neural lineage differentiation markers defined by previous studies (23), and among these 28 genes, 23 are OPC or oligodendrocyte markers. This finding suggests that EGF-dependent *Cic*-regulated differentiation genes are predominantly related to oligodendrocyte lineage differentiation. The genes in the second group (group II, 183 genes) are EGFR-regulated but not Cic-related targets, which display differential

expression change in response to EGF depletion (EGF− vs. EGF+) but not affected by *Cic* status ($Cic^{-/-}$ vs. $Cic^{+/+}$). This finding supports the notion that *Cic* is only one of the downstream mediators of the EGFR signaling pathway. Most interestingly, the genes in the third and largest group of genes (group III, 192 genes) display a very different differential expression pattern from the above two groups—they are not affected by EGF in either $Cic^{+/+}$ or $Cic^{-/-}$ NSCs, but display differential expression in $Cic^{-/-}$ versus $Cic^{+/+}$ NSCs, suggesting they are non EGF-regulated Cic targets. Therefore, this group represents a previously unrecognized, non EGFR-controlled role of Cic. Collectively, these results support that Cic does act as one downstream mediator of the EGFR signal as previously reported; however, there is a major, novel part of Cic function that is not regulated by EGFR signaling and has not been thoroughly investigated (Fig. 4B).

Genes whose expression is affected by *Cic* loss are involved in a variety of cellular processes (Supplementary Table S3), highlighting a broad and essential role of Cic in NSCs. In particular, in the presence of EGF (as in an actual tumorigenic condition), Gene Set Enrichment Analysis (GSEA) (45,46) revealed that in the context of Cic loss, the most affected gene set was that of oxidative phosphorylation (Fig. 4C). This suggests a likely reduced use of the tricarboxylic acid (TCA) cycle in the $Cic^{-/-}$ NSCs, thus providing an explanation for the mild hypoxia-specific propagation advantage of these cells. In further supporting the oncogenic role of *Cic* knockout, $Cic^{-/-}$ NSCs also display down-regulated expression of multiple genes with tumor suppressor function (e.g., *Erdr1*, *F2rl1*, *Sparch1*, and *Ajap1*), and increased expression of oncogenes (e.g., *Hoxa1*, *Wnt5a*, and *Sostdc1*) (Supplementary Table S2). Collectively, these results suggest that loss of *Cic* does not simply resemble a constitutive activation of the EGFR signaling pathway, and support the existence of an EGFR-independent oncogenic effect of *Cic* loss.

Cic loss leads to downregulated expression of a set of genes and dictates a unique gene expression signature in human ODs

In analyzing differential gene expression, we noted that regardless of the absence or presence of EGF, there were more genes that were downregulated than genes that were upregulated in $Cic^{-/-}$ NSCs (104 upregulated vs. 88 downregulated, Supplementary Table S2). Although this can be due to an indirect effect, it is nevertheless unexpected, as Cic is believed to function as a transcriptional suppressor (13–15,17,19,20). To test whether this result is specific only to NSCs, we investigated the effect of *CIC* knockout in a human OD cell line, HOG (24). We designed sgRNAs targeting human *CIC* and utilized the CRISPR/Cas9 gene editing to obtain four isogenic *CIC*-knockout HOG cell lines (Supplementary Figs. S7A). Knocking out of the *CIC* was validated both by genomic sanger sequencing and western blot (Supplementary Figs. S7B and S7C) Global gene expression analysis revealed that again in the HOG model, *CIC* deletion induced differential expression of 154 genes (identified by the cutoff of ≥2 fold or ≤0.5 fold). Most remarkably, 90% (139 out of 154) of these genes were down-regulated upon *CIC* knockout (Supplementary Table S4).

Anti-CIC ChIP-seq analysis of HOG cell lines identified a large number of loci that were directly bound by CIC (Fig. 5A; Supplementary Table S5). Combined with the HOG microarray data, it appears that among differentially expressed genes bound by CIC, 83%

(68 out of 82) of them displayed down-regulated expression upon *CIC* knockout (examples in Fig. 5B; Supplementary Fig. S8; and Supplementary Table S5). Collectively, and together with findings from the NSC models, these results support the notion that in addition to the established transcriptional suppression activity that is regulated by EGFR signaling, CIC likely also functions in the positive regulation of gene transcription.

Finally, to fully evaluate the effect of *CIC*'s absence on the transcriptional landscape in ODs, we expanded this gene expression correlation analysis onto a larger set of genes that demonstrated significant differential expression between the *CIC* mutant versus *CIC* wild type group of ODs reported by the TCGA studies. We selected ODs with IDH1 mutations to ensure a more meaningful comparison and segregated ODs into those with *CIC*-intact ($CIC^{+/+}$), with heterozygous *CIC* loss (1p/19q deletion with *CIC* wild type, designated as $CIC^{+/-}$), and with homozygous *CIC* mutations (1p/19q deletion with *CIC* mutations, designated as $CIC^{-/-}$). We again found an expression signature that is unique to the $CIC^{-/-}$ group while the other two groups of ODs ($CIC^{+/+}$ and $CIC^{+/-}$) displayed non-distinguishable gene expression signatures (Fig. 5C). It is worth noting that again 60% (452 out of 748) of those differentially expressed genes are downregulated when Cic is lost. Although ODs with *CIC* mutations exclusively fall into the group of ODs that carry deletion of 1p/19q, the chromosomal loss does not explain the unique gene expression signature displayed in the $CIC^{-/-}$ group, as those differentially expressed genes are located across the genome (Supplementary Fig. S9). Together, these results suggest that while the effects of loss of one copy of *CIC* (via deletion or chromosomal 19q loss) are more difficult to assess, the complete absence of functional *CIC* defines a unique gene expression signature in ODs.

CIC loss potentiates tumorigenesis in a *PDGFB*-driven orthotopic glioma model

The difficulty in obtaining homozygous knockout animals presents a problem for monitoring the long-term effects on tumorigenesis *in vivo*. Bearing in mind the established two-hit hypothesis in driving tumorigenesis (i.e., a loss of a tumor suppressor and the gain-of-function of an oncogene), we alternatively sought to determine the effect of *Cic* loss in the context of aberrant oncogenic signaling. Here, we utilized *ex vivo* culture of NSCs followed by subsequent orthotopic implantation. We adapted a well-characterized mouse model of OD that is driven by *PDGFB*, one of the most common and well-established oncogenes in glioma and one that was previously shown to induce glioma-resembling ODs (47,48). P4 $Cic^{flox/flox}$ or control $Cic^{+/+}$ NSCs were harvested and transduced with Cre-expressing adenovirus to remove the loxP-flanked exons to generate $Cic^{-/-}$ or control $Cic^{+/+}$ NSCs. The resultant NSCs were transduced with *PDGFB*-expressing retrovirus and implanted into the right striatum of immunocompromised Nod scid gamma (NSG) mice (Fig. 6A). Mice were sacrificed when they showed signs or symptoms of brain abnormalities such as macrocephaly or lethargy. We observed that the $Cic^{+/+}$, *PDGFB*-expressing NSCs gave rise to tumors with a median survival of 167 days. Remarkably, in the animals implanted with $Cic^{-/-}$, *PDGFB*-expressing NSCs, the tumors displayed a shorter latency with a significantly shorter median survival of 129 days (log-rank $p<0.01$) (Fig. 6B). Consistent with the previous study (47), both $Cic^{+/+}$ and $Cic^{-/-}$ *PDGFB*-expressing NSCs gave rise to low-grade, infiltrating tumors. Interestingly, compared to the tumors derived from $Cic^{+/+}$ NSCs, the $Cic^{-/-}$ NSC-derived tumors displayed less dense cellularity, lower mitotic activity, and

less vascular proliferation. Additionally, the *Cic*$^{-/-}$ NSC-derived tumors had a decreased propensity to infiltrate the subarachnoid space and form plaque-like tumors, and were more likely to exhibit features found in ODs, including perivascular and perineuronal satellitosis, and perinuclear cytoplasmic halos (Fig. 6C). Collectively, these results support that *Cic* loss potentiates gliomagenesis and facilitates the development of tumors with OD characteristics.

Discussion

In this study, we provided evidence showing that *Cic* ablation causes aberrant development of NSCs and neural lineage cells in the SVZ, compromises NSC differentiation (in particularly to the oligodendrocyte lineage), confers NSC EGF-independent proliferation, and promotes tumorigenesis in an orthotopic glioma model.

In our conventional *Cic* knockout (*Cic*$^{null/null}$) mouse models, although the difficulty in obtaining homozygous knockout animals presents a challenge for studying early neurogenesis in depth, the abnormalities in the SVZ of those viable *Cic*$^{null/null}$ pups were obvious. The SVZ is a heterogeneous reservoir of NSCs and neural progenitor cells, and is at its maximum size at birth when the immature brain is at a dynamic state of development and undergoing active neurogenesis (49). We observed proliferative cells in the SVZ of both *Cic*$^{null/null}$ and *Cic*$^{+/+}$ neonatal mice. This is indicative of an active and comparable neurogenesis with or without the presence of Cic, likely suggesting that the transcriptional suppression role of Cic was blocked at this stage. However, at P28, when the mouse brain is at a mature state and active neurogenesis is not expected, the continuous presence of Ki67 positive cells was still observed in the SVZ of *Cic*$^{null/null}$ mice, but not in *Cic*$^{+/+}$ mice, suggesting the presence of aberrant proliferative signaling in the adult mouse SVZ when *Cic* is absent. One prominently proliferative population in the developing brain is the GFAP-expressing type B radial cells, which are believed to be multipotent NSCs (40). This enlarged GFAP positive radial cell population in the SVZ, and the thickening of the lateral walls of the SVZ in the *Cic*$^{null/null}$ adult mice compared to that of the control wildtype adult mice, likely indicate an aberrant hyper-proliferative activity in the adult SVZ. Although the exact identity of cell lineages that are most susceptible to *Cic* loss-driven OD remains to be determined, these results provide direct evidence to support a role of *Cic* ablation in inducing aberrant cell proliferation and elucidate the tumor suppressive role of *Cic.*

Our mechanistic studies lead to two intriguing insights regarding the biochemical roles of *Cic* and its tumor suppressor role. First, previous studies using drosophila models suggest Cic functions as downstream mediator of EGFR signaling. Generally, certain downstream genes can only be transcribed when EGFR signaling is activated; the loss of *Cic* leads to the absence of this suppression and results in these genes being actively transcribed independent of EGFR-mediated activation, thus equating the loss of *Cic* to an activation of EGFR signaling. However, our results suggest that *Cic* loss is distinguishable from EGF-dependent activation of EGFR signaling pathway, and more likely leads to a cascade of events that are not entirely regulated by the EGFR pathway. Interestingly, we found that in both our mouse NSC and the human cell line model, a large number of genes bound by CIC actually displayed reduced expression when *CIC* was absent, thus raising an intriguing possibility that CIC may indeed function as a transcriptional activator under some circumstances.

Second, in the NSC model, the compensation of *Cic* knockout for the absence of EGF, as assayed by NSC propagation, was only obvious when cells were cultured under mild hypoxic conditions. While we did not directly assess the situation in an *in vivo* condition, it suggests a link between *Cic* knockout and hypoxia, as mild hypoxia is an intrinsic component to both physiological neurogenesis and pathogenic processes such as tumorigenesis (41,42). Interestingly, a previous study in *Drosophila* showed that *cic* is one of the three genes that when knocked down, lead to significantly improved hypoxia tolerance (50). Our finding also raises a possibility that *Cic* status is a factor for consideration when designing therapeutics based on intervention with hypoxic pathways. Further studies in NSCs and in additional tumor models will be necessary to illustrate the interplay between Cic function and the mild hypoxic microenvironments, and the therapeutic implication.

The tumor suppressor function of Cic is further underscored by the broad scope of genes that display differential expression upon *Cic* knockout, including the upregulation of potential oncogenes and the downregulation of those with tumor suppressive roles. This is consistent with recent studies indicating that CIC mutations are associated with a more aggressive subtype in ODs (51,52). Among these Cic-regulated genes, the ones that are essential in mediating the pathogenic role of *Cic* deletion are still unclear. One intriguing candidate is *Ajap1*, which is involved in numerous cellular processes associated with tumorigenesis and is frequently lost or epigenetically silenced in gliomas (53,54). Further studies are needed to determine key downstream mediator genes, among numerous other downstream genes identified as differentially expressed in the $Cic^{-/-}$ cells, which are responsible for the tumorigenic role of *Cic* loss.

Our *in vivo* gliomagenesis modeling study raises several important questions. First, it remains to be determined which specific populations/lineages of cells are most susceptible to *Cic* deletion-driven transformation. Second, it is noted that although we used *PDGFB* as an oncogenic driver for the current study to illustrate the tumorigenic role of the *Cic* deletion, it is almost certain that *CIC* deletion can cooperate with multiple genetic alterations in driving ODs, including those mutations co-occurrent with *CIC* mutations, such as the *IDH1/2* mutations (6,7). In this regard, it is also noted that the HOG cell line that was used in the current study, while initially derived from an OD patient, lacks the IDH1/2 mutations and 1p/19q co-deletion (24,55). Our results should therefore be interpreted in the context of this limitation, and future studies using more genetically representative human OD cell models may be necessary to further define the role of CIC in OD. Finally, it is notable that *Cic* deletion can potentiate gliomagenesis that is driven by PDGFR signaling, which is itself a potent oncogenic driver for gliomas (47,48). As PDGF receptor kinase inhibitors, e.g., imatinib, have been under active development as a strategy for glioma treatment, future studies will be required to determine how the status of CIC affects tumor cell response to such inhibitors. The *Cic* knockout mouse and cell line models (as described in the current study) provide valuable tools for addressing these questions.

Supplementary Material

Refer to Web version on PubMed Central for supplementary material.

Acknowledgments

Financial support: This work was supported by National Cancer Institute grant R01CA140316 (to H.Yan). Y.He was supported by an American Association for Cancer Research (AACR)-Aflac Career Development Award (grant number 13-20-10-HE), a National Comprehensive Cancer Network Young Investigator Award, and the Circle of Service Foundation.

We thank Cheryl Bock of Duke Transgenic and Knockout Mouse Shared Resource for generating the knockout mouse models, Duke Sequencing and Genomic Technologies Shared Resource for performing the microarray experiments and sequencing for ChIP samples, and David Corcoran of Duke Genomic Analysis and Bioinformatics Shared Resource for ChIP-seq data analysis. We thank Jenna Lewis for editorial revisions to the manuscript.

References

1. Ostrom QT, Gittleman H, Fulop J, Liu M, Blanda R, Kromer C, et al. CBTRUS Statistical Report: Primary Brain and Central Nervous System Tumors Diagnosed in the United States in 2008–2012. Neuro-oncology. 2015; 17(Suppl 4):iv1–iv62. [PubMed: 26511214]
2. Bromberg JE, van den Bent MJ. Oligodendrogliomas: molecular biology and treatment. The oncologist. 2009; 14:155–63. [PubMed: 19182242]
3. Maintz D, Fiedler K, Koopmann J, Rollbrocker B, Nechev S, Lenartz D, et al. Molecular genetic evidence for subtypes of oligoastrocytomas. Journal of neuropathology and experimental neurology. 1997; 56:1098–104. [PubMed: 9329453]
4. Smith JS, Perry A, Borell TJ, Lee HK, O'Fallon J, Hosek SM, et al. Alterations of chromosome arms 1p and 19q as predictors of survival in oligodendrogliomas, astrocytomas, and mixed oligoastrocytomas. Journal of clinical oncology : official journal of the American Society of Clinical Oncology. 2000; 18:636–45. [PubMed: 10653879]
5. Suzuki H, Aoki K, Chiba K, Sato Y, Shiozawa Y, Shiraishi Y, et al. Mutational landscape and clonal architecture in grade II and III gliomas. Nature genetics. 2015; 47:458–68. [PubMed: 25848751]
6. Jiao Y, Killela PJ, Reitman ZJ, Rasheed AB, Heaphy CM, de Wilde RF, et al. Frequent ATRX, CIC, FUBP1 and IDH1 mutations refine the classification of malignant gliomas. Oncotarget. 2012; 3:709–22. [PubMed: 22869205]
7. Bettegowda C, Agrawal N, Jiao Y, Sausen M, Wood LD, Hruban RH, et al. Mutations in CIC and FUBP1 contribute to human oligodendroglioma. Science. 2011; 333:1453–5. [PubMed: 21817013]
8. Sahm F, Koelsche C, Meyer J, Pusch S, Lindenberg K, Mueller W, et al. CIC and FUBP1 mutations in oligodendrogliomas, oligoastrocytomas and astrocytomas. Acta neuropathologica. 2012; 123:853–60. [PubMed: 22588899]
9. Yip S, Butterfield YS, Morozova O, Chittaranjan S, Blough MD, An J, et al. Concurrent CIC mutations, IDH mutations, and 1p/19q loss distinguish oligodendrogliomas from other cancers. The Journal of pathology. 2012; 226:7–16. [PubMed: 22072542]
10. Brat DJ, Verhaak RG, Aldape KD, Yung WK, Salama SR, et al. Cancer Genome Atlas Research N. Comprehensive, Integrative Genomic Analysis of Diffuse Lower-Grade Gliomas. The New England journal of medicine. 2015; 372:2481–98. [PubMed: 26061751]
11. Killela PJ, Reitman ZJ, Jiao Y, Bettegowda C, Agrawal N, Diaz LA Jr, et al. TERT promoter mutations occur frequently in gliomas and a subset of tumors derived from cells with low rates of self-renewal. Proceedings of the National Academy of Sciences of the United States of America. 2013; 110:6021–6. [PubMed: 23530248]
12. Lee CJ, Chan WI, Cheung M, Cheng YC, Appleby VJ, Orme AT, et al. CIC, a member of a novel subfamily of the HMG-box superfamily, is transiently expressed in developing granule neurons. Brain research Molecular brain research. 2002; 106:151–6. [PubMed: 12393275]
13. Jimenez G, Guichet A, Ephrussi A, Casanova J. Relief of gene repression by torso RTK signaling: role of capicua in Drosophila terminal and dorsoventral patterning. Genes & development. 2000; 14:224–31. [PubMed: 10652276]
14. Kawamura-Saito M, Yamazaki Y, Kaneko K, Kawaguchi N, Kanda H, Mukai H, et al. Fusion between CIC and DUX4 up-regulates PEA3 family genes in Ewing-like sarcomas with t(4;19)(q35;q13) translocation. Human molecular genetics. 2006; 15:2125–37. [PubMed: 16717057]

15. Astigarraga S, Grossman R, Diaz-Delfin J, Caelles C, Paroush Z, Jimenez G. A MAPK docking site is critical for downregulation of Capicua by Torso and EGFR RTK signaling. The EMBO journal. 2007; 26:668–77. [PubMed: 17255944]
16. Fores M, Simon-Carrasco L, Ajuria L, Samper N, Gonzalez-Crespo S, Drosten M, et al. A new mode of DNA binding distinguishes Capicua from other HMG-box factors and explains its mutation patterns in cancer. PLoS genetics. 2017; 13:e1006622. [PubMed: 28278156]
17. Roch F, Jimenez G, Casanova J. EGFR signalling inhibits Capicua-dependent repression during specification of Drosophila wing veins. Development. 2002; 129:993–1002. [PubMed: 11861482]
18. Lohr U, Chung HR, Beller M, Jackle H. Antagonistic action of Bicoid and the repressor Capicua determines the spatial limits of Drosophila head gene expression domains. Proceedings of the National Academy of Sciences of the United States of America. 2009; 106:21695–700. [PubMed: 19959668]
19. Ajuria L, Nieva C, Winkler C, Kuo D, Samper N, Andreu MJ, et al. Capicua DNA-binding sites are general response elements for RTK signaling in Drosophila. Development. 2011; 138:915–24. [PubMed: 21270056]
20. Lam YC, Bowman AB, Jafar-Nejad P, Lim J, Richman R, Fryer JD, et al. ATAXIN-1 interacts with the repressor Capicua in its native complex to cause SCA1 neuropathology. Cell. 2006; 127:1335–47. [PubMed: 17190598]
21. Skarnes WC, Rosen B, West AP, Koutsourakis M, Bushell W, Iyer V, et al. A conditional knockout resource for the genome-wide study of mouse gene function. Nature. 2011; 474:337–42. [PubMed: 21677750]
22. Huang da W, Sherman BT, Lempicki RA. Systematic and integrative analysis of large gene lists using DAVID bioinformatics resources. Nature protocols. 2009; 4:44–57. [PubMed: 19131956]
23. Zhang Y, Chen K, Sloan SA, Bennett ML, Scholze AR, O'Keeffe S, et al. An RNA-sequencing transcriptome and splicing database of glia, neurons, and vascular cells of the cerebral cortex. The Journal of neuroscience : the official journal of the Society for Neuroscience. 2014; 34:11929–47. [PubMed: 25186741]
24. Post GR, Dawson G. Characterization of a cell line derived from a human oligodendroglioma. Molecular and chemical neuropathology. 1992; 16:303–17. [PubMed: 1329795]
25. Ran FA, Hsu PD, Wright J, Agarwala V, Scott DA, Zhang F. Genome engineering using the CRISPR-Cas9 system. Nature protocols. 2013; 8:2281–308. [PubMed: 24157548]
26. Doench JG, Fusi N, Sullender M, Hegde M, Vaimberg EW, Donovan KF, et al. Optimized sgRNA design to maximize activity and minimize off-target effects of CRISPR-Cas9. Nature biotechnology. 2016; 34:184–91.
27. Hsu PD, Scott DA, Weinstein JA, Ran FA, Konermann S, Agarwala V, et al. DNA targeting specificity of RNA-guided Cas9 nucleases. Nature biotechnology. 2013; 31:827–32.
28. Mavrakis KJ, McDonald ER 3rd, Schlabach MR, Billy E, Hoffman GR, deWeck A, et al. Disordered methionine metabolism in MTAP/CDKN2A-deleted cancers leads to dependence on PRMT5. Science. 2016; 351:1208–13. [PubMed: 26912361]
29. Guo C, Chang CC, Wortham M, Chen LH, Kernagis DN, Qin X, et al. Global identification of MLL2-targeted loci reveals MLL2's role in diverse signaling pathways. Proceedings of the National Academy of Sciences of the United States of America. 2012; 109:17603–8. [PubMed: 23045699]
30. Langmead B, Trapnell C, Pop M, Salzberg SL. Ultrafast and memory-efficient alignment of short DNA sequences to the human genome. Genome biology. 2009; 10:R25. [PubMed: 19261174]
31. Zhang Y, Liu T, Meyer CA, Eeckhoute J, Johnson DS, Bernstein BE, et al. Model-based analysis of ChIP-Seq (MACS). Genome biology. 2008; 9:R137. [PubMed: 18798982]
32. Robinson JT, Thorvaldsdottir H, Winckler W, Guttman M, Lander ES, Getz G, et al. Integrative genomics viewer. Nature biotechnology. 2011; 29:24–6.
33. Thorvaldsdottir H, Robinson JT, Mesirov JP. Integrative Genomics Viewer (IGV): high-performance genomics data visualization and exploration. Briefings in bioinformatics. 2013; 14:178–92. [PubMed: 22517427]
34. Huang W, Loganantharaj R, Schroeder B, Fargo D, Li L. PAVIS: a tool for Peak Annotation and Visualization. Bioinformatics. 2013; 29:3097–9. [PubMed: 24008416]

35. Pear WS, Miller JP, Xu L, Pui JC, Soffer B, Quackenbush RC, et al. Efficient and rapid induction of a chronic myelogenous leukemia-like myeloproliferative disease in mice receiving P210 bcr/abl-transduced bone marrow. Blood. 1998; 92:3780–92. [PubMed: 9808572]
36. Gao J, Aksoy BA, Dogrusoz U, Dresdner G, Gross B, Sumer SO, et al. Integrative analysis of complex cancer genomics and clinical profiles using the cBioPortal. Science signaling. 2013; 6:pl1. [PubMed: 23550210]
37. Cerami E, Gao J, Dogrusoz U, Gross BE, Sumer SO, Aksoy BA, et al. The cBio cancer genomics portal: an open platform for exploring multidimensional cancer genomics data. Cancer discovery. 2012; 2:401–4. [PubMed: 22588877]
38. Ceccarelli M, Barthel FP, Malta TM, Sabedot TS, Salama SR, Murray BA, et al. Molecular Profiling Reveals Biologically Discrete Subsets and Pathways of Progression in Diffuse Glioma. Cell. 2016; 164:550–63. [PubMed: 26824661]
39. Tanaka A, Watanabe Y, Kato H, Araki T. Immunohistochemical changes related to ageing in the mouse hippocampus and subventricular zone. Mechanisms of ageing and development. 2007; 128:303–10. [PubMed: 17316762]
40. Doetsch F, Caille I, Lim DA, Garcia-Verdugo JM, Alvarez-Buylla A. Subventricular zone astrocytes are neural stem cells in the adult mammalian brain. Cell. 1999; 97:703–16. [PubMed: 10380923]
41. Erecinska M, Silver IA. Tissue oxygen tension and brain sensitivity to hypoxia. Respiration physiology. 2001; 128:263–76. [PubMed: 11718758]
42. Ljungkvist AS, Bussink J, Kaanders JH, van der Kogel AJ. Dynamics of tumor hypoxia measured with bioreductive hypoxic cell markers. Radiation research. 2007; 167:127–45. [PubMed: 17390721]
43. Cahoy JD, Emery B, Kaushal A, Foo LC, Zamanian JL, Christopherson KS, et al. A transcriptome database for astrocytes, neurons, and oligodendrocytes: a new resource for understanding brain development and function. The Journal of neuroscience : the official journal of the Society for Neuroscience. 2008; 28:264–78. [PubMed: 18171944]
44. Emery B, Agalliu D, Cahoy JD, Watkins TA, Dugas JC, Mulinyawe SB, et al. Myelin gene regulatory factor is a critical transcriptional regulator required for CNS myelination. Cell. 2009; 138:172–85. [PubMed: 19596243]
45. Subramanian A, Tamayo P, Mootha VK, Mukherjee S, Ebert BL, Gillette MA, et al. Gene set enrichment analysis: a knowledge-based approach for interpreting genome-wide expression profiles. Proc Natl Acad Sci U S A. 2005; 102:15545–50. [PubMed: 16199517]
46. Mootha VK, Lindgren CM, Eriksson KF, Subramanian A, Sihag S, Lehar J, et al. PGC-1alpha-responsive genes involved in oxidative phosphorylation are coordinately downregulated in human diabetes. Nature genetics. 2003; 34:267–73. [PubMed: 12808457]
47. Dai C, Celestino JC, Okada Y, Louis DN, Fuller GN, Holland EC. PDGF autocrine stimulation dedifferentiates cultured astrocytes and induces oligodendrogliomas and oligoastrocytomas from neural progenitors and astrocytes in vivo. Genes & development. 2001; 15:1913–25. [PubMed: 11485986]
48. Uhrbom L, Hesselager G, Nister M, Westermark B. Induction of brain tumors in mice using a recombinant platelet-derived growth factor B-chain retrovirus. Cancer Res. 1998; 58:5275–9. [PubMed: 9850047]
49. Buono KD, Goodus MT, Guardia Clausi M, Jiang Y, Loporchio D, Levison SW. Mechanisms of mouse neural precursor expansion after neonatal hypoxia-ischemia. The Journal of neuroscience : the official journal of the Society for Neuroscience. 2015; 35:8855–65. [PubMed: 26063918]
50. Udpa N, Ronen R, Zhou D, Liang J, Stobdan T, Appenzeller O, et al. Whole genome sequencing of Ethiopian highlanders reveals conserved hypoxia tolerance genes. Genome biology. 2014; 15:R36. [PubMed: 24555826]
51. Chan AK, Pang JC, Chung NY, Li KK, Poon WS, Chan DT, et al. Loss of CIC and FUBP1 expressions are potential markers of shorter time to recurrence in oligodendroglial tumors. Modern pathology : an official journal of the United States and Canadian Academy of Pathology, Inc. 2014; 27:332–42.

52. Gleize V, Alentorn A, Connen de Kerillis L, Labussiere M, Nadaradjane AA, Mundwiller E, et al. CIC inactivating mutations identify aggressive subset of 1p19q codeleted gliomas. Ann Neurol. 2015; 78:355–74. [PubMed: 26017892]

53. McDonald JM, Dunlap S, Cogdell D, Dunmire V, Wei Q, Starzinski-Powitz A, et al. The SHREW1 gene, frequently deleted in oligodendrogliomas, functions to inhibit cell adhesion and migration. Cancer biology & therapy. 2006; 5:300–4. [PubMed: 16410724]

54. Lin N, Di C, Bortoff K, Fu J, Truszkowski P, Killela P, et al. Deletion or epigenetic silencing of AJAP1 on 1p36 in glioblastoma. Molecular cancer research : MCR. 2012; 10:208–17. [PubMed: 22241217]

55. Reitman ZJ, Jin G, Karoly ED, Spasojevic I, Yang J, Kinzler KW, et al. Profiling the effects of isocitrate dehydrogenase 1 and 2 mutations on the cellular metabolome. Proc Natl Acad Sci U S A. 2011; 108:3270–5. [PubMed: 21289278]

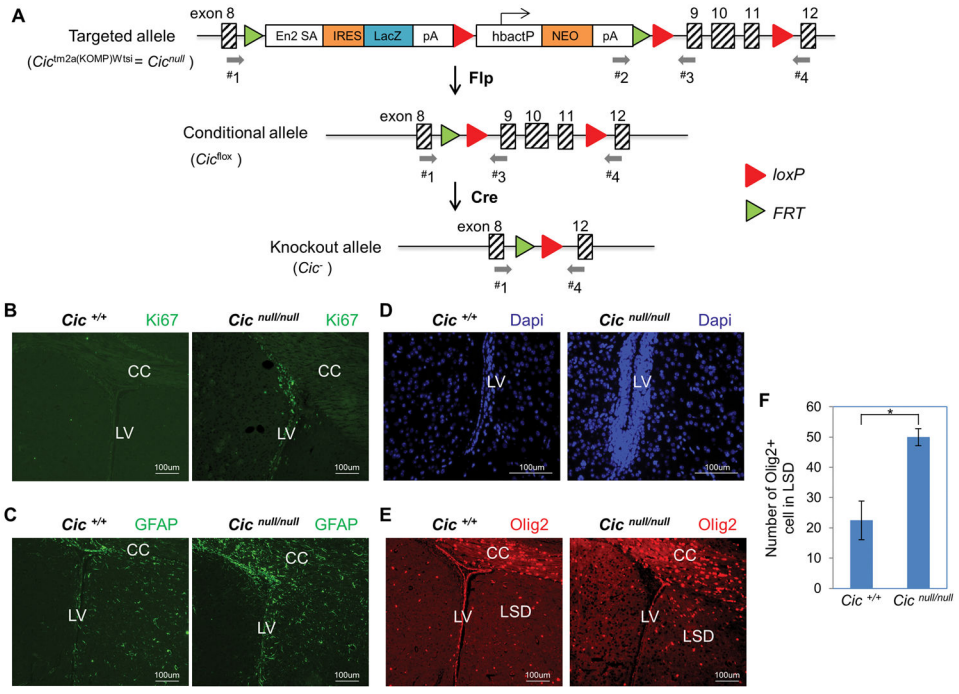

Figure 1.

Cic knockout results in aberrant hyper-proliferative cells in adult SVZ. **A,** *Cic* knockout strategy. A gene trap cassette flanked by FRT sites was inserted between Cic exon 8 and 9, and exon 9, 10 and 11 were flanked by loxP sites. When treated with Flp recombinase, the gene trap cassette can be removed, resulting in a conditional allele (Cic function is restored). This conditional allele can be further converted into a knockout allele by deleting exon 9,10 and 11 via Cre recombinase. Grey arrows represent genotyping primers. **B–E,** Representative immunofluorescent stained FFPE slides from similar planes of postnatal day 28 (P28) $Cic^{+/+}$ (n=2) and $Cic^{null/null}$ (n=2) mouse brains for the following markers: **B,** Ki67 (10X), **C,** GFAP (10X), **D,** Dapi (20X), and **E,** Olig2 (10X). **F,** Quantifications of Olig2+ cells as shown in (E). Abbreviations: mouse En2 splicing acceptor (En2 SA), internal ribosome entry site (IRES), LacZ reporter (LacZ) and the SV40 polyadenylation sequences (pA), human b-actin promoter (hbactP), corpus callosum (CC); lateral ventricle (LV); lateral septal nucleus (LSD).

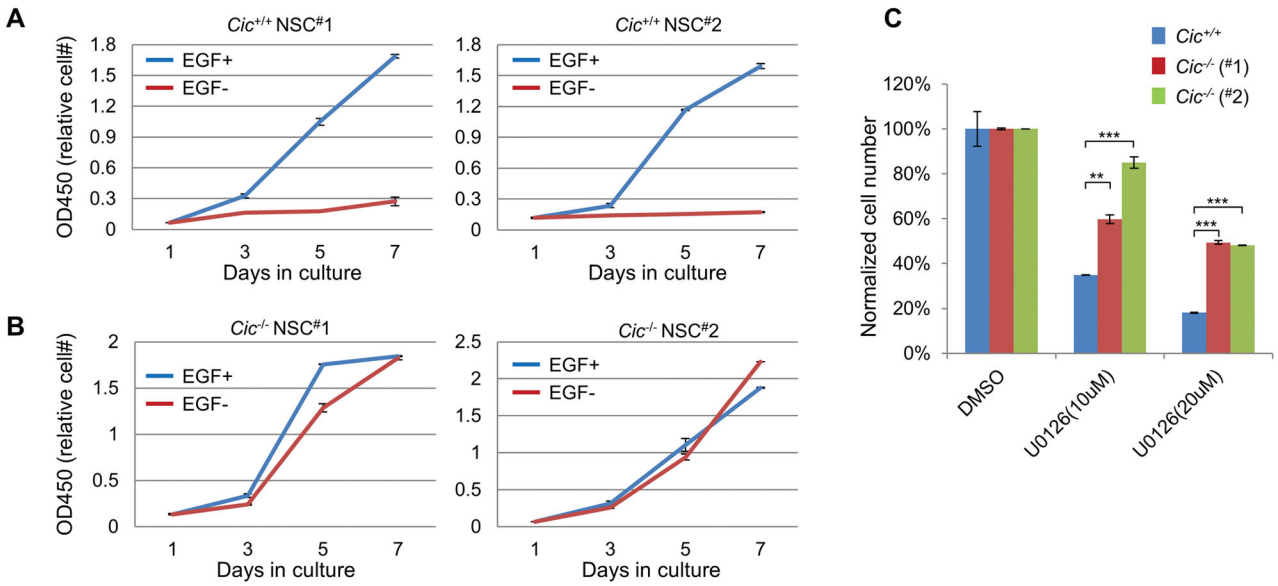

Figure 2.

Cic knockout confers EGFR signaling-independent propagation of NSCs. **A**, Propagation of two $Cic^{+/+}$ NSC lines under mild hypoxic culture condition (3% oxygen) and with or without EGF. **B**, Propagation of two $Cic^{-/-}$ NSC lines under the same experimental condition as (A). **C**, Propagation of $Cic^{+/+}$ and $Cic^{-/-}$ NSC lines in the presence of U0126 for 5 days. Cell numbers of each cell line were normalized to their DMSO treated controls.

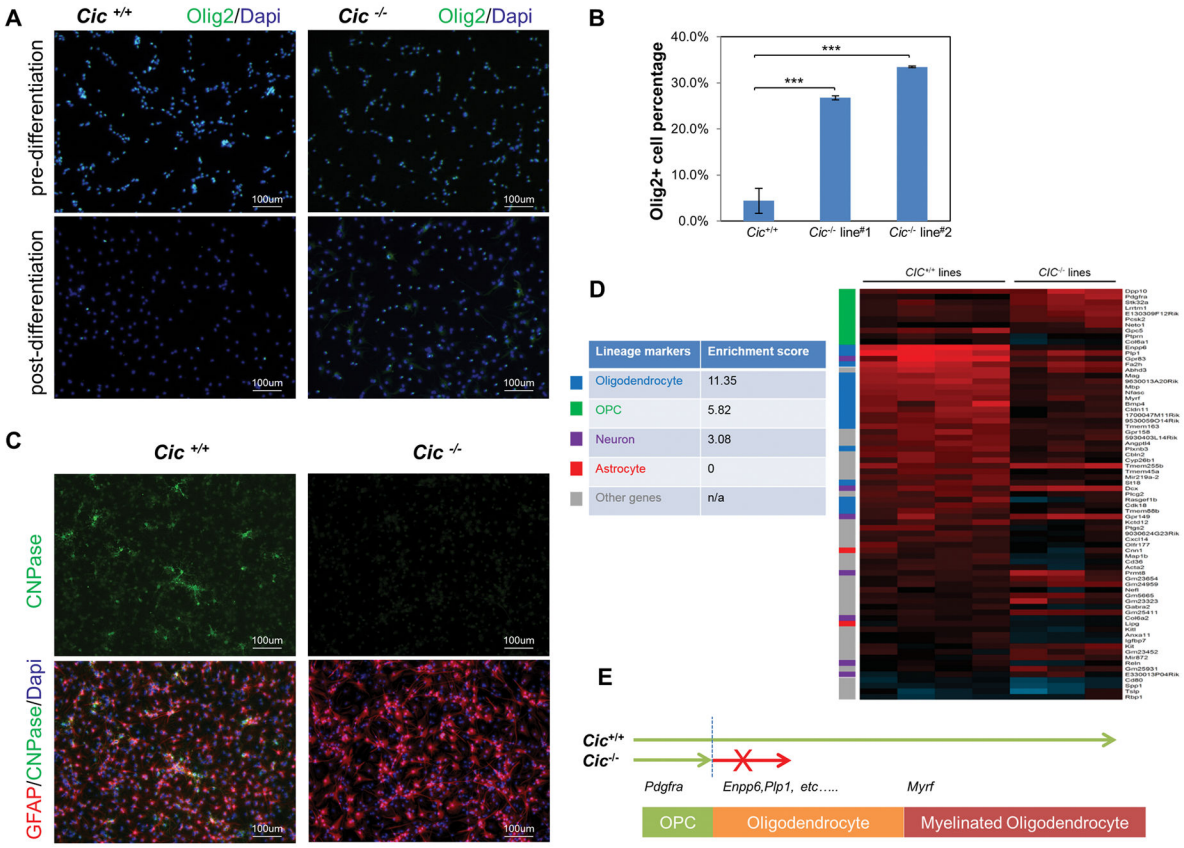

Figure 3.

Cic$^{-/-}$ NSCs fail to differentiate into mature oligodendrocyte and are arrested in an OPC-like state. *Cic*$^{+/+}$ and *Cic*$^{-/-}$ NSCs were maintained in the standard proliferation media or in differentiation medium for seven days. Immunofluorescent staining was performed. **A,** Staining (10X) for Olig2 and Dapi. **B,** Quantification of Olig2+ cells upon differentiation in (A). Three randomly-chosen fields were quantified for each cell line (two-tailed t-test analysis). **C,** Post-differentiation staining (10X) for GFAP and CNPase and counterstained with Dapi. **D,** Most differentially expressed genes in *Cic*$^{-/-}$ versus *Cic*$^{+/+}$ NSCs in response to EGF depletion. Each column represents fold change (EGF− vs.EGF+) of gene expression for a sample. Positive value (red) represents higher expression in EGF-depleted condition compared to in EGF-supplemented condition. Genes defined as different neural lineage markers are color-coded at the left. Enrichment scores (−log(p-value or EASE score)) were calculated for each lineage marker (see method for details). **E,** A proposed schematic for *Cic* loss-induced compromised oligodendrocyte differentiation.

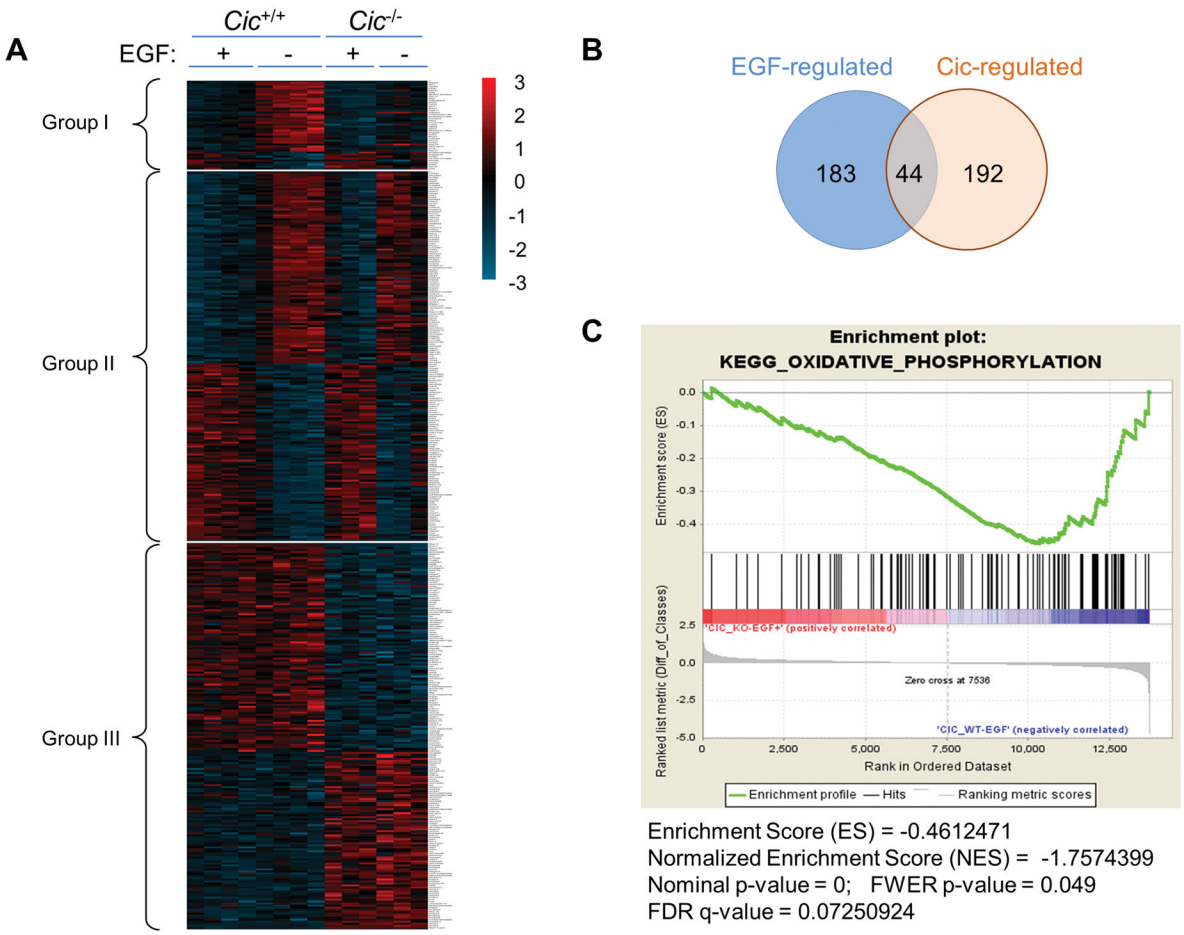

Figure 4.

Cic and EGFR signaling regulate overlapping yet distinct groups of genes. **A**, three groups of genes that are distinctly regulated by EGF and by Cic. **B**, Venn diagram shows overlapping genes (group I, 44 genes) between EGF downstream targets (227 genes) and Cic downstream targets (236 genes). **C**, GSEA analysis of mRNA profiles revealed downregulated oxidative phosphorylation as the top pathway altered in *Cic*$^{-/-}$ NSCs.

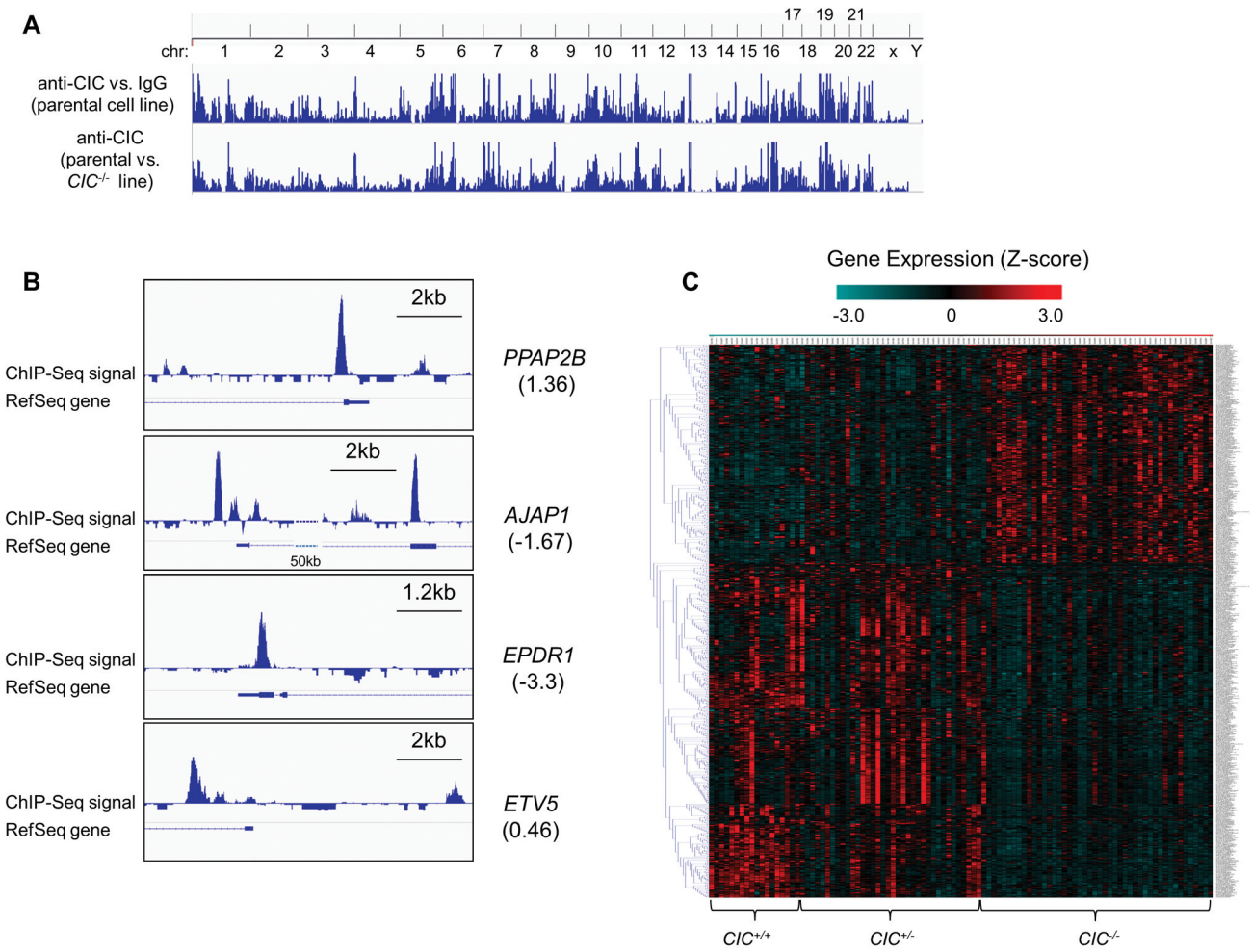

Figure 5.

Genes bound by CIC displayed both up- and down-regulated expression in CIC-null cells. **A**, Genome-wide CIC binding loci identified by comparing anti-CIC ChIP-Seq to a control IgG ChIP-Seq signals in the parental HOG cells (top panel), or by comparing anti-CIC ChIP-seq in the parental HOG cell line to anti-CIC ChIP-seq in an isogenic *CIC*$^{-/-}$ HOC derivative line as the negative control (bottom panel). **B**, Signal tracks show CIC binding sites for *AJAP1, EPDR1, ETV5, PPAP2B* genes. Statistically significant peaks were identified in regions of transcriptional start site (TSS) (for *EPDR1, PPAP2B, AJAP1*), promoter (for *ETV5*), intron (for *ETV5*) and exon (for *AJAP1*). Numbers in parentheses following the gene symbols indicate fold change (log2 ratio) of gene expression (KO vs. parental). **C,** RNA-seq data analysis of TCGA OD patients. *CIC*$^{-/-}$ tumors displayed a unique expression signature that is distinct from either *CIC*$^{+/+}$ or *CIC*$^{+/-}$ tumors (748 genes, 100 patients).

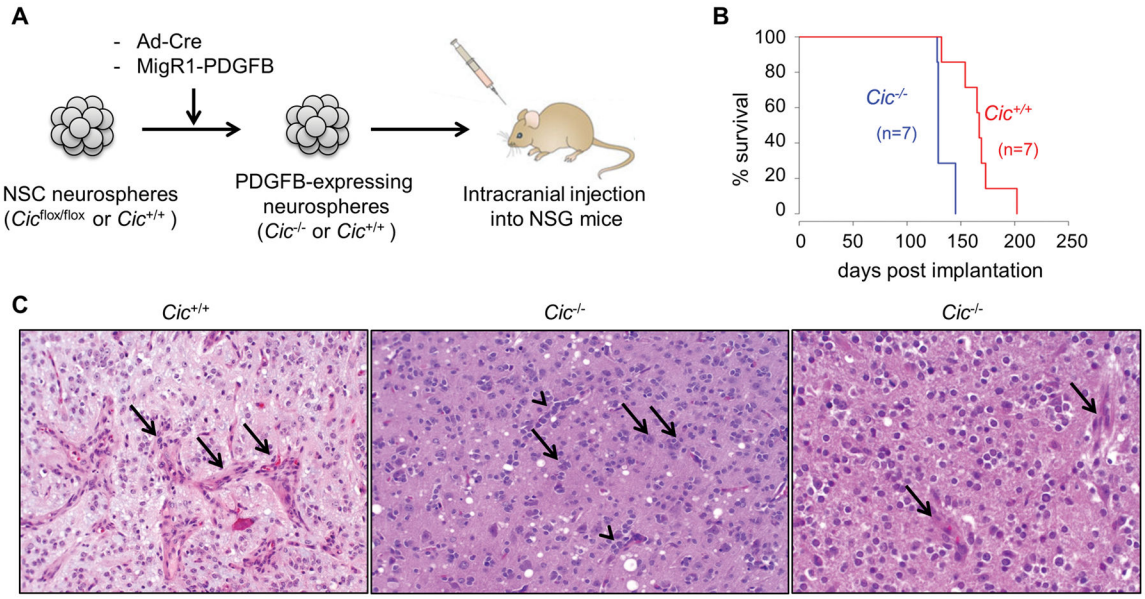

Figure 6.

Cic deletion potentiates *PDGFB*-driven gliomagenesis. **A**, *PDGFB*-expressing NSCs with genotype of either $Cic^{+/+}$ or $Cic^{-/-}$ were implanted into the right cortex of 4–6 weeks old NSG mice (n=7 for each cell line). **B**, Kaplan-meier analysis revealed that *Cic* deletion event in *PDGFB*-expressing NSCs was associated with a shorter median survival of implanted animals when compared to the wild type control group (129 days Vs 167 days, log-rank test p=0.0013). **C**, H&E staining of xenograft sections: (left, 40X) vascular proliferation in $Cic^{+/+}$ tumors (arrows); (middle, 20X) perivascular satellitosis (arrowheads) and perineuronal satellitosis (arrows) in $Cic^{-/-}$ tumors; (right, 40X) perinuclear halos and bland vessels that lack evidence of proliferation (arrows) in $Cic^{-/-}$ tumors.